Environmental Science & Technology

pubs.acs.org/est

Article

Quantifying Mercury Distribution and Source Contribution in Surface Soil of Qinghai-Tibetan Plateau Using Mercury Isotopes

Nantao Liu, Xinyuan Cai, Longyu Jia, Xun Wang,* Wei Yuan, Che-Jen Lin, Dingyong Wang, and Xinbin Feng

Cite This: *Environ. Sci. Technol.* 2023, 57, 5903−5912

Read Online

ACCESS | Metrics & More | Article Recommendations | Supporting Information

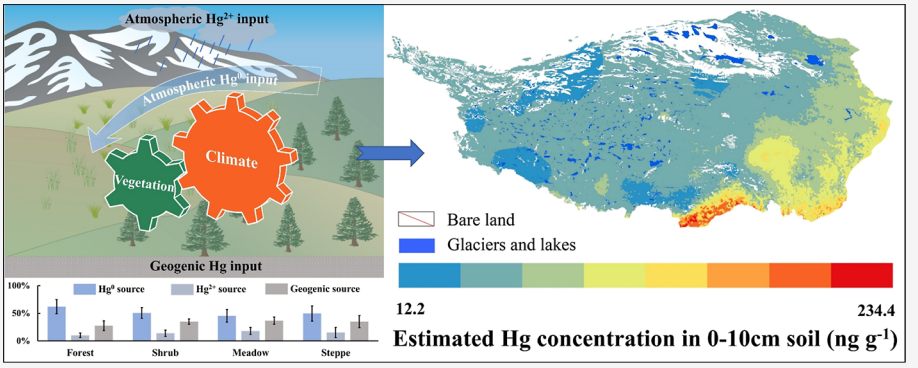

ABSTRACT: Long-range transport and atmospheric deposition of gaseous mercury (Hg^0) result in significant accumulation of Hg in the Qinghai-Tibetan Plateau (QTP). However, there are significant knowledge gaps in understanding the spatial distribution and source contribution of Hg in the surface soil of the QTP and factors influencing Hg accumulation. In this study, we comprehensively investigated Hg concentrations and isotopic signatures in the QTP to address these knowledge gaps. Results show that the average Hg concentration in the surface soil ranks as follows: forest (53.9 ± 36.9 ng g^{-1}) > meadow (30.7 ± 14.3 ng g^{-1}) > steppe (24.5 ± 16.1 ng g^{-1}) > shrub (21.0 ± 11.6 ng g^{-1}). Hg isotopic mass mixing and structural equation models demonstrate that vegetation-mediated atmospheric Hg^0 deposition dominates the Hg source in the surface soil, with an average contribution of 62 ± 12% in forests, followed by 51 ± 10% in shrub, 50 ± 13% in steppe, and 45 ± 11% in meadow. Additionally, geogenic sources contribute 28−37% of surface soil Hg accumulation, and atmospheric Hg^{2+} inputs contribute 10−18% among the four types of biomes. The Hg pool in 0−10 cm surface soil over the QTP is estimated as 8200 ± 3292 Mg. Global warming, permafrost degradation, and anthropogenic influences have likely perturbed Hg accumulation in the soil of QTP.

KEYWORDS: *mercury, isotopes, source apportionment, surface soil, Qinghai-Tibetan Plateau*

1. INTRODUCTION

Mercury (Hg) is a global pollutant with 6000−8000 Mg annual emissions into air from anthropogenic and natural sources, which are subsequently transported by atmospheric circulation and deposited in remote terrestrial ecosystems.[1,2] Hg accumulation in remote terrestrial ecosystems has generated ecological and health concerns globally. Known as "The Third Pole" of the world, the Qinghai-Tibetan Plateau (QTP) is a pristine region in the Northern Hemisphere at an average altitude of more than 4000 m above the sea level and far away from anthropogenic sources.[3] Elevated Hg accumulation has been recently found in some anthropogenically impacted surface soils of the QTP up to 1 order of magnitude higher than the background soil Hg concentration in other remote areas.[4−10] These findings have suggested that the local climate, vegetation, and geomorphological characteristics all influence the process of Hg accumulation in surface soil.[4,6−8,11] However, the spatial variation, source contribution, and controlling factors for the observed Hg accumulation over the QTP remain unclear due to the scarcity of synthesized observational data and direct evidence.

Vegetation-induced atmospheric Hg^0 deposition is the predominant pathway of Hg accumulation in most low-lying terrestrial biomes.[12−16] For example, ≥80% of Hg accumulated in forest soils is derived from vegetative uptake of atmospheric Hg^0 followed by litterfall deposition.[17,18] Whether such a vegetation-induced atmospheric Hg^0 deposition controls Hg

Received: December 21, 2022
Revised: February 27, 2023
Accepted: March 16, 2023
Published: March 28, 2023

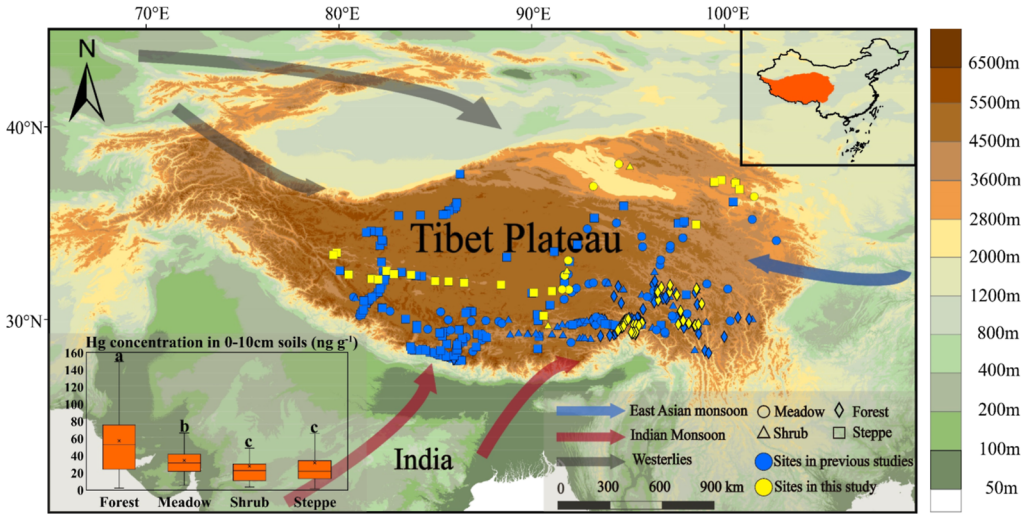

Figure 1. Sampling sites considered in this study. The yellow dots represent the sample sites in this study, and the blue dots represent the sites from earlier studies.[5,6,10,23] The box chart shows the variation of Hg concentrations in the surface soil of forest, shrub, meadow, and steppe. The different letters in the box chart suggest a significant difference at 95% confidence level.

accumulation in the QTP remains to be confirmed, given its unique climate and topographic features. The moisture of Indian monsoon brings precipitation to the southeastern QTP, leading to the intensive forest cover.[19] As the Indian monsoon weakens from the southeast to northwest of the QTP, strong influences of the westerly result in a dry and cold climate at the high-elevation regions of the northwestern QTP, forming thin vegetation covers of the alpine steppe.[20] The distinct water, wind, and glacial erosions over the QTP[21,22] also cause unique rock weathering processes and geogenic Hg accumulation, depending on local environmental conditions.[23] Furthermore, the boundary transport across the Himalayas moves air parcels containing elevated concentration of atmospheric Hg from South Asia that subsequently deposits in the southern QTP.[5,24] Similar effects caused by the Indian monsoon and Eastern Asian monsoon also increase the deposition of atmospheric Hg originated from the inner regions of China and Southeast Asia.[25−27] Thus, understanding the Hg accumulation and sources over the QTP requires measurements capable of detecting source-specific signals.

Stable Hg isotope techniques, including Hg mass-dependent fractionation (MDF) and mass-independent fractionation (MIF), provide a new tool for tracing the sources of Hg stored in environmental samples.[28,29] Important isotopic endmembers of Hg for air, rock, litter, and rainfall samples have been documented with their unique Hg isotopic fingerprints over the QTP.[6,24,30,31] Biogeochemical cycles of Hg in ecosystems also exhibit isotopic transition signals that can be quantified by MDF and MIF values. MIF of odd isotopes (odd-MIF, reported as Δ^{199}Hg and Δ^{201}Hg) mainly occurs in the Hg biogeochemical processes of photo-reduction[32−35] and dark redox reactions.[33,36] MIF of even isotopes (even-MIF, reported as Δ^{200}Hg and Δ^{204}Hg) is caused by the photo-oxidation of Hg^0 in the troposphere, with positive values observed in precipitation.[37,38] These analytical fingerprints enable identification of the transformation, source, and fate of Hg in terrestrial biomes over the QTP.

In this study, we hypothesize that the unique climatic and topographic conditions in the QTP develop unique vegetation covers that control the spatial Hg accumulation in surface soil. We applied the data describing Hg isotopic signatures of surface soil and associated information regarding landcovers of forest, shrub, steppe, and meadow to illustrate Hg sources and accumulation processes in surface soil. Factors controlling the spatial distribution over the QTP are also discussed. Statistical models were applied to understand the influences of environmental and climatic conditions on Hg distribution in the surface soil. The special distribution of Hg stored in the surface soils over the QTP is developed. Finally, we discussed the response of Hg accumulation in surface soils to the climate change in the QTP.

2. METHODOLOGY

2.1. Site Description. The QTP (26°00′−39°47′N, 73°19′−104°47′E) hosts an area of approximately 2.5 × 10^6 km^2 and an average altitude of more than 4000 m a.s.l (Figure 1). The climate over QTP is characterized by reduced air pressure, high UV irradiance, and low temperature with an annual average ranging from −4.9 to 6.1 °C. The precipitation decreases from the southeast (600−800 mm yr^{-1}) to the northwest (200−400 mm yr^{-1}). Various vegetation covers are found in the QTP due to the combined effects of natural factors (climate, topography, etc.) and biological adaptability. There are four primary types of vegetation covers over the QTP, including forest, meadow, steppe, and shrub, of which forest has the highest vegetation biomass, followed by meadow, shrub, and steppe. The dominant vegetation species vary largely, depending on the local natural factors. For example, the dominant vegetation species in alpine forests are *Picea likiangensis*, *Abies georgei*, *Abies spectabilis*, and *Larix potaninii*; and *Rhododendron nivale*, *Rhododendron beesianum*, *Quercus guyavifolia*, and *Juniperus squamata* in alpine shrubs.

2.2. Sample Collection. Surface soil samples from 80 carefully selected sites in the QTP were collected from 2018 to 2020, including 49 forest samples, 8 meadow samples, 3 shrub samples, and 20 steppe samples. In addition, we reviewed the Hg data of approximately 397 sites from previous studies (Figure 1).[5,6,10,23] The distances among sampling sites range from 20 to 300 km based on the vegetation covers and the terrains, with the locations of sampling sites shown in Figure 1. To avoid potential seasonal effects, all samples were collected in July and August only. The detailed sampling protocols have

https://doi.org/10.1021/acs.est.2c09610
Environ. Sci. Technol. 2023, 57, 5903−5912

been described in previous studies.[6,10] In brief, each sampling site was selected to cover 150 m of nearly flat land surface and without human activities, except for minor grazing activities in some meadow and grassland areas. We then set three to five 5 × 5 m quadrats at each sampling site to collect 0−10 cm topsoil. Within each quadrat, five replicate soil samples were collected in an "S" shape and mixed to form one sample (mass of approximately 1−2 kg). The coefficient of variation of Hg concentration during the sampling follows the distribution of Figure S1.

After collection, the soil samples were placed in a cool and dark room for air drying then ground with an agate mortar, sieved through a 200 mesh (74 μm) nylon screen, and finally placed in a polyethylene bag for chemical analysis. We have shown that air-drying causes little change in the Hg concentration and isotopic compositions in the soil samples.[6,39] To prevent cross-contamination during sample preparation, the grinding tools and screens were rinsed with purified water and then dried with ethanol wipes after each sample.

2.3. Chemical Analysis. Hg concentrations of soil samples were measured by using a DMA-80 Hg analyzer. We determined Hg concentrations of one certified soil reference material and one parallel sample in every nine samples. The recovery of certified soil reference material (GSS-5, Hg concentration: 290 ± 30 ng g^{-1}) ranged from 95 to 105%. The bias of the parallel sample was less than 5%. In addition, we used the Walkley-back method to measure soil organic carbon (SOC). In brief, this method uses $Cr_2O_7^{2-}$ to oxidize SOC and then reduces the excess $Cr_2O_7^{2-}$ by $FeSO_4$ to calculate the SOC content.[40]

Preconcentration of Hg in soil samples and determination of Hg isotopic compositions have been described in our earlier work.[6,31] The spatial distribution of soil samples selected for Hg isotopic composition analysis was showed in Figure S2. The selected soil samples were processed by double-stage heating pyrolysis in a tube muffle furnace. The Hg vapor from the sample was then captured by using 5 mL of 40% reverse aqua regia (HCl/HNO_3 = 1:3, v/v) trapping solution.[41] The Hg concentration enriched in the trapping solution was measured by cold vapor atomic fluorescence spectrometry (Tekran 2500) following the US-EPA method 1631 (detection limit is 0.5 ng L^{-1}).[42] The pre-concentration recovery was in the range of 93−104%. The Hg isotopic compositions were determined by a multi-collector inductively coupled plasma mass spectrometer (MC ICP−MS, Nu-Plasma II, Thermo Scientific). The trapping solution was diluted to 0.5 ng mL^{-1} and imported into the gas−liquid separator together with 3% $SnCl_2$ solution. From Bergquist and Blum,[35] the Hg MDF is reported as

$$\delta^{202}\mathrm{Hg}\ (‰) = 1000 \times [(^{202}\mathrm{Hg}/^{198}\mathrm{Hg}_{\mathrm{sample}}) / (^{202}\mathrm{Hg}/^{198}\mathrm{Hg}_{\mathrm{NIST\text{-}3133}}) - 1] \quad (1)$$

where $(^{202}\mathrm{Hg}/^{198}\mathrm{Hg}_{\mathrm{NIST\text{-}3133}})$ represents the isotopic ratio in the standard sample (NIST-3133).

MIF is calculated as

$$\Delta^{199}\mathrm{Hg}\ (‰) = \delta^{199}\mathrm{Hg} - 0.2520 \times \delta^{202}\mathrm{Hg} \quad (2)$$

$$\Delta^{200}\mathrm{Hg}\ (‰) = \delta^{200}\mathrm{Hg} - 0.5024 \times \delta^{202}\mathrm{Hg} \quad (3)$$

$$\Delta^{201}\mathrm{Hg}\ (‰) = \delta^{201}\mathrm{Hg} - 0.7520 \times \delta^{202}\mathrm{Hg} \quad (4)$$

To evaluate whether isotopic composition bias occurs pre-concentration, we determined the Hg isotopic compositions of a certified soil reference material GSS-4. Results of GSS-4 were δ^{202}Hg = −1.84 ± 0.34‰, Δ^{199}Hg = −0.42 ± 0.063‰, Δ^{201}Hg = −0.41 ± 0.05‰, and Δ^{200}Hg = −0.02 ± 0.08‰ (mean ± 2σ, n = 6). The NIST-8610 standard solution was measured every 10−15 samples as a secondary standard with results as δ^{202}Hg = −0.52 ± 0.11‰, Δ^{199}Hg = −0.01 ± 0.08‰, Δ^{201}Hg = −0.04 ± 0.05‰, and Δ^{200}Hg = −0.03 ± 0.05‰ (mean ± 2σ, n = 28). These measured values were consistent with the reported results,[43−45] indicating negligible isotopic bias.

2.4. Data Analysis. Soil Hg concentrations reported in peer-review literature are shown in Figure 1. Given the various soil depths in the studies (e.g., 0−5 cm and 0−15 cm depth), a weighted factor was applied to normalize the Hg concentration values to 0−10 cm depth. The weighted factor was determined from results of Hg distribution in soil profiles at 25 sites over the QTP.[46] In addition, data sets of annual precipitation,[47] normalized difference vegetation index (NDVI),[48] net primary productivity (NPP),[49] and soil bulk density[50] over the QTP were obtained from the Tibetan Plateau Science Data Center.

We then mapped the spatial distribution of Hg concentration in the 0−10 cm surface soil over the QTP by a cokriging spatial interpolation modeling by ArcMap 10.7. We utilized a random process and an optimal linear unbiased estimation in the cokriging spatial interpolation modeling based on the cross-validation results of semi-variogram, which is developed to determine the degree of spatial continuity of the target variable as follows

$$\gamma_{ij}(h) = \frac{1}{2N(h)} \sum_{n=1}^{Z(h)} [Z_i(x_n) - Z_i(x_n + h)] [Z_j(x_n) - Z_j(x_n + h)] \quad (5)$$

where $\gamma_{ij}(h)$ is the cross-semivariance of two random variables as a function of h. $N(h)$ is the number of pairs of $Z_i(x)$ and $Z_j(x)$ at a separate distance h. To further estimate the distribution of soil Hg storage over the QTP, all data were re-gridded into a 0.1° × 0.1° grid cell. The 0−10 cm surface soil Hg storage is estimated as

$$\mathrm{Hg}_{\mathrm{storage}} = \mathrm{Hg}_{\mathrm{con}} \times \text{bulk density} \times \text{depth} \quad (6)$$

where $\mathrm{Hg}_{\mathrm{con}}$ is the average Hg concentration (ng g^{-1}) and bulk density is the bulk density of soil (g m^{-3}) in each grid cell; depth refers to the 0.1 m soil depth in this study.

The IBM SPSS Statistics v25.0 and R Studio were used for statistical analysis at 95% confidence level. We used one-way ANOVA and post hoc Tukey HSD to conduct the significant difference analysis when data were normally distributed. Otherwise, the Kruskal−Wallis test was applied. Pearson correlation analysis was applied to evaluate the relation between different variables. We also used principal component analysis (PCA) to extract the first principal components of NDVI and NPP to represent the proxy index of vegetation biomass (Supporting Information for details). Finally, a structural equation model (SEM) was developed based on the χ^2 test with maximum likelihood estimation to quantify impacts of the environmental and climatic factors on soil Hg accumulation over the QTP. More details for the setup of the SEM are described in our earlier studies.[45,51] From the SEM pathway network, the normalized path coefficient (β)

https://doi.org/10.1021/acs.est.2c09610
Environ. Sci. Technol. 2023, 57, 5903−5912

represents the direct influence of one variable on another, and the indirect influence is calculated by multiplying each associated β.

3. RESULTS AND DISCUSSION

3.1. Hg Distribution in Surface Soils of the QTP. The average Hg concentration in 0−10 cm surface soil in the QTP is 31.8 ± 34.9 ng g^{-1} (mean ± SD, median = 29.0 ng g^{-1}, 1.3−237.5 ng g^{-1}, Table S1), comparable to the earlier reported values (37.0 ± 18.0 ng g^{-1}; $P > 0.05$, by t-test).[23] The terrestrial biomes significantly influence surface soil Hg concentration ($P < 0.01$, one-way ANOVA, Figure 1), with the highest values found for forest (53.9 ± 36.9 ng g^{-1}), followed by meadow (30.7 ± 14.3 ng g^{-1}), steppe (24.5 ± 16.1 ng g^{-1}), and shrub (21.0 ± 11.6 ng g^{-1}). The Hg concentrations are significantly lower than those found in low-elevation regions for similar biomes (e.g., 77.9 ± 65.4 ng g^{-1} in 0−10 cm forest soils in southwestern China[12] and 138 ± 15 ng g^{-1} in tundra soils of Arctic Alaska[13]). This can be attributed to the extreme climatic and environmental conditions, remote from anthropogenic influences and high-mountain barrier in the QTP, that lead to the low atmospheric Hg depositions. For example, the total atmospheric Hg deposition flux ranging among 5.1−7.9 μg m^{-2} yr^{-1} at the QTP sites, while up to ∼102.8 μg m^{-2} yr^{-1} in forests of the southwestern China and ∼9.2 μg m^{-2} yr^{-1} in Arctic tundra.[13,52,53]

3.2. Factors Influencing Hg Accumulation in Surface Soils of the QTP. The Hg concentration in 0−10 cm surface soil shows the highest positive correlation to the SOC content, followed by NDVI and precipitation, and then to latitude and longitude (Figure S3) at 95% confidence level. Earlier studies attributed the increasing Hg concentration with the elevation to enhanced atmospheric Hg deposition at select sites of high altitude.[4,54] We found significant correlation between surface soil Hg concentration and altitude in the forest soil samples (Figure S4). However, the correlation became weaker when the entire samples in the QTP were considered (Figure S3). This is likely caused by the local climate that induces spatial heterogeneities, variations among different types of vegetation, and changes in the geographical environment among regions over a larger spatial scale.

The SEM results display the impacts of spatial parameters (latitude and longitude) and environmental factors (precipitation, vegetation biomass, and SOC) on soil Hg variation in the QTP (Figure 2), which can explain 52% of the variation in the Hg concentration in 0−10 cm surface soil. The SOC has the greatest direct effect (β = 0.56), followed by precipitation (β = 0.26). The direct positive effect of precipitation reflects the atmospheric Hg^{2+} inputs controlled by precipitation intensity.[55−57] The SOC mainly comes from the decomposition of litterfall,[46] and its turnover is affected by climatic conditions such as precipitation and temperature[58,59] Thus, the direct effect of SOC on soil Hg concentration reflects the atmospheric Hg^0 deposition by vegetation uptake and incorporation of atmospheric Hg by SOC through complexation between SOC and Hg in surface soil.[60,61] The significant β values of latitude/longitude-precipitation/vegetation in Figure 2 indicate that latitude and longitude have indirect effects on soil Hg by spatial variability of precipitation, vegetation biomass, and SOC.

3.3. Source Attribution Estimated by Stable Hg Isotope Evidence. The isotopic compositions of Hg in

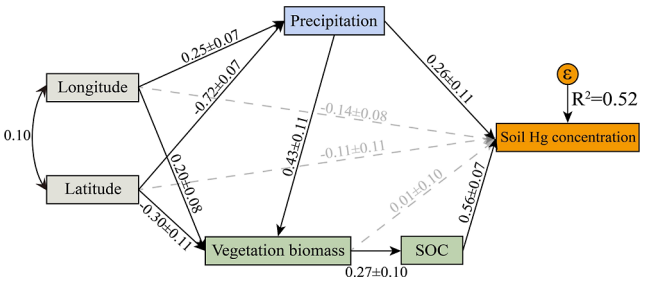

Figure 2. SEM fitted to surface soil Hg concentration among longitude, latitude, precipitation, vegetation biomass, and SOC. Solid arrows indicate significant effects at 95% confidence level, while gray arrows and numbers indicate insignificant effects. The numbers are normalized path coefficients (β) and their standard errors, indicating the direct influence of one variable on the other.

surface soil vary among terrestrial biomes (Figure 3A,B). The soil δ^{202}Hg for forest shows the most negative values (mean = −1.44 ± 0.51‰), followed by shrub (−1.03 ± 0.39‰), meadow (−0.92 ± 0.34‰), and then steppe (−0.91 ± 0.69‰). The Δ^{199}Hg values in forest soil are most negative (−0.14 ± 0.14‰), similar to those found in total gaseous Hg^0 in air (−0.20 ± 0.08‰)[24] and litter of the QTP forests (−0.18 ± 0.09‰).[6] This is strong evidence that forest soil is of atmospheric origin.[15,16,31,62] Comparable values are found among the samples of meadow (0.05 ± 0.11‰), shrub (0.00 ± 0.13‰), and steppe (−0.05 ± 0.14‰). The Δ^{200}Hg values in all soil samples are close to 0.00‰. The more negative δ^{202}Hg values in forest soil ($P < 0.01$, one-way ANOVA) than in other biomes are caused by a greater production of biomass in forest foliage that facilitates atmospheric Hg^0 uptake and litter deposition, since the lighter Hg isotopes are preferentially taken up by vegetation (e.g., a shift of ∼−2.8‰ δ^{202}Hg between foliage and air Hg).[15,63]

Three source endmembers (Figure 3C,D) have been identified for Hg in the soil surface in the QTP, including atmospheric Hg^0 uptake, Hg^{2+} deposition by precipitation, and geogenic sources (i.e., weathering process-induced rock Hg release into soil).[15,16,31,62] Geogenic sources have a relatively lower Hg concentration (several to 10 ng g^{-1}) and negative δ^{202}Hg and close 0 Δ^{199}Hg values.[1,64,65] The atmospheric Hg^0 sources mediated by vegetation and soil direct uptake show negative Δ^{199}Hg values and elevated SOC and soil Hg concentrations. The Δ^{199}Hg in the surface soil of the QTP decreases with increasing Hg concentration (Figure 3E), suggesting the important role of atmospheric Hg^0 uptake by foliage and direct deposition into soil. Nevertheless, the soil samples with the low Hg concentrations in meadow and steppe have positive Δ^{199}Hg values (up to 0.20‰). This cannot be explained by the mixing of atmospheric Hg^0 and geogenic input. Precipitation in the QTP shows positive Δ^{200}Hg (0.20 ± 0.05‰) and a Δ^{199}Hg value (0.95 ± 0.14‰) significantly higher than typical values across the globe (0.47 ± 0.39‰).[13,15,37,38] Though the soil samples exhibit insignificant Δ^{200}Hg signals (−0.02 ± 0.05‰) in meadow and steppe, the highly positive Δ^{199}Hg values of precipitation suggest that even a small contribution of atmospheric Hg^{2+} input can cause a positive shift of Δ^{199}Hg in surface soils. The slope of Δ^{199}Hg to Δ^{201}Hg at 1.07 (Figure 3F) indicates that Hg accumulated in soil has undergone photochemical processes before.[1,65]

Hg biogeochemical processes in terrestrial ecosystems can shift the MIF values in soil samples. Even-MIF occurs mainly

https://doi.org/10.1021/acs.est.2c09610
Environ. Sci. Technol. 2023, 57, 5903−5912

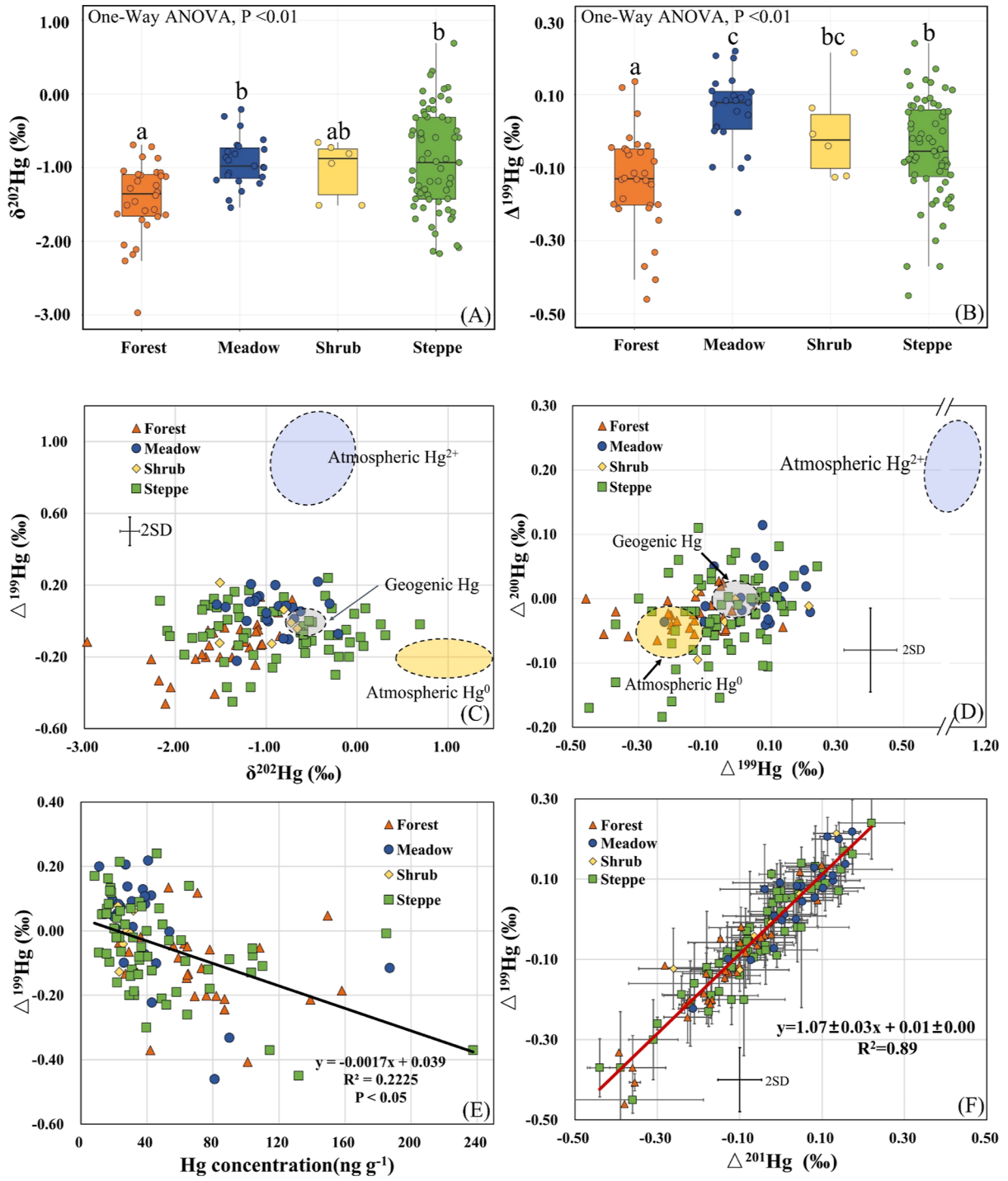

Figure 3. Hg isotopic signatures and correlations. (A) δ^{202}Hg values in surface soil, (B) Δ^{199}Hg values in surface soil; (C) Δ^{199}Hg versus δ^{202}Hg in surface soil; (D) Δ^{200}Hg versus Δ^{199}Hg in surface soil; (E) Δ^{199}Hg versus Hg concentration in surface soil; (F) Δ^{201}Hg versus Δ^{199}Hg in surface soil from four vegetation types. The different letters in the box chart suggest a significant difference at a 95% confidence level. The error bar represents ±2 standard deviation.

during photo-oxidation of Hg^0 in the troposphere.[37,38] Photochemical reactions in surface soil induces a Δ^{199}Hg shift too small to account for the significant shift of sources mixing over the QTP.[1,46,65] Hence, we used Δ^{200}Hg and Δ^{199}Hg in the three-endmember mixing model to trace the surface soil Hg sources. Earlier studies have reported the Δ^{199}Hg and Δ^{200}Hg signatures for atmospheric Hg^0 input in the QTP at −0.20 ± 0.04 and −0.06 ± 0.02‰,[24] for atmospheric Hg^{2+} at 0.95 ± 0.14 and 0.20 ± 0.05‰,[62] and for geogenic Hg at −0.02 ± 0.05, and 0.01 ± 0.01‰,[31,46] respectively. These values were used in this study. The detailed model configuration is described in the Supporting Information.

The results of Hg isotopic mixing modeling highlight the dominant role of atmospheric Hg^0 input in controlling Hg accumulation in surface soil (Figure 4A). The highest contribution of atmospheric Hg^0 input is in forest (62 ± 12%), followed by shrub (51 ± 10%), steppe (50 ± 13%), and

https://doi.org/10.1021/acs.est.2c09610
Environ. Sci. Technol. 2023, 57, 5903−5912

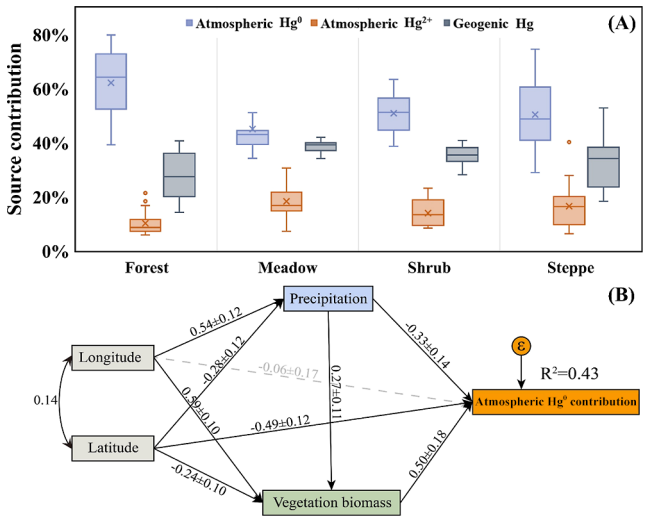

Figure 4. Hg source attribution and SEM results. (A) Contribution of atmospheric Hg^0, atmospheric Hg^{2+}, and geogenic sources in the surface soil; (B) structural equation modeling fitted to the atmospheric Hg^0 contribution among longitude, latitude, precipitation, and vegetation biomass. Solid arrows and numbers indicate a significant direct effect, while gray arrows and numbers indicate an insignificant effect at a 95% confidence level. The numbers are normalized path coefficients (β) and their standard errors, indicating the direct influence of one variable on the other.

then meadow (45 ± 11%). The contribution of atmospheric Hg^{2+} input in forest, meadow, shrub, and steppe is 10 ± 4, 18 ± 6, 14 ± 6, and 18 ± 8%, respectively. Additionally, geogenic sources contribute 28 ± 9% of Hg accumulation in forest, 35 ± 5% in shrub, 35 ± 11% in steppe, and 37 ± 7% in meadow. Atmospheric Hg^0 contribution significantly correlates to soil Hg concentration and NDVI, while the soil Hg concentration anticorrelates to geogenic Hg contribution (Figure S5). These relations confirm that greater biomass production increases atmospheric Hg^0 accumulation in surface soil.

The factors influencing spatial distribution of the atmospheric Hg^0 contribution over the QTP were analyzed by the SEM (Figure 4B). The precipitation has a significant negative effect on the variation of atmospheric Hg^0 contribution (β = −0.33). This is caused by the relatively consistent contribution of geogenic source at all sites (28−37% in Figure 4A), and therefore, the increase of Hg^{2+} contribution would reduce the contribution of atmospheric Hg^0 in Hg isotopic mixing model. Vegetation biomass has the greatest direct effect on the contribution of atmospheric Hg^0 input (β = 0.50) as expected. Interestingly, latitude has a significant negative effect on the contribution of atmospheric Hg^0 (β = −0.49). This means that soil at lower altitude tends to accumulate more Hg mass, possibly caused by transboundary transport of atmospheric Hg from South/Southeast Asia.[3,5,24,66] Additionally, the significant β values of latitude-vegetation in Figure 4B indicate that latitude has an indirect effect on atmospheric Hg^0 accumulation in soil by influencing the spatial variability of vegetation distribution. The forest in low-altitude regions shows much stronger atmospheric Hg^0 deposition through the vegetation uptake (Figure S6).

Due to the similar Δ^{200}Hg signatures between geogenic sources and atmospheric Hg^0 and the ∼0 value of Δ^{199}Hg in geogenic sources, the Hg isotopic mixing model could produce an artifact in estimating the contribution of geogenic Hg sources. To reduce modeling uncertainties, we updated the Hg isotopic mixing model by considering a two-stage binary mixing model (more details in the Supporting Information). The Hg isotopic signatures of an endmember depend on the source type and location. Hence, uncertainties may arise by setting a constant value for each endmember. In addition, the Hg-MIF shifts induced by the Hg biogeochemical processes after deposition may also introduce additional uncertainties. For example, photo- and SOC-reduction in surface soil of meadow and steppe could lead to a shift of odd-MIF.[46,67,68] The photoreduction on forest floor is relatively weaker than that in meadow and steppe because of intensive canopy shading.[1] Our earlier work shows that coupling the Hg isotope mixing model with Monte Carlo simulations effectively quantifies the uncertainties of model results.[31] These uncertainties are quantified by generating one million groups of MIF signatures randomly ranging from mean − SD to mean + SD to solve the Hg isotope mixing model. Uncertainties range from 24 to 32% (2SD) depending on the local biome types. Using Hg/Ti ratios and Δ^{200}Hg signatures, an earlier study estimated a 40−55% atmospheric Hg^0 deposition in surface soils of meadow and steppe.[46] Our estimation is consistent with the earlier observations, confirming the source contribution to the surface soil of the QTP.

3.4. Mapping Surface Soil Hg Storage over the QTP.

Considering the predominant role of vegetation in controlling Hg accumulation, the spatial distribution of Hg storage in surface soil of 0−10 cm depth (Figure 5) is developed using a cokriging spatial interpolation model based on the relation between the soil Hg concentration and vegetation biomass production (i.e., NPP). The scatterplot of model-predicted versus observed Hg concentration yields a slope of 0.7 (R^2 = 0.69, P < 0.01), indicating that the applied methodology adequately captures the magnitude and spatial variation of observed Hg concentrations in the QTP.

The soil Hg concentration and storage of 0−10 cm depth both show a decreasing trend from the southeast to northwest of the QTP (Figure 5), showing gradient from higher soil Hg concentrations in forested area to lower concentrations in the mid-west and northern areas covered by steppe. The total Hg pool in 0−10 cm surface soil over the QTP is estimated to be 8200 ± 3292 Mg, including 1246 ± 518 Mg in forest soil, 2763 ± 1095 Mg in meadow soil, 885 ± 357 Mg in shrub soil, and 2943 ± 1186 Mg in steppe soil. Due to the large areal coverage, Hg storage in the 0−10 cm surface soils in steppe and meadow accounts for 36% and 34%, respectively. Our earlier study showed a transition of foliage to root uptake of Hg along with increasing elevation in the QTP and estimated that 30 ± 19% Hg in permafrost foliage is from foliage uptake of atmospheric Hg^0, 31 ± 17% from root uptake of previously deposited Hg^0, 16 ± 15% from root uptake of previously deposited Hg^{2+}, and 23 ± 20% from root uptake of previously geogenic Hg.[46] This suggests that the large Hg storage in the meadow and steppe in the permafrost region has a longer accumulation time scale compared to the forested regions.

The sparse spatial coverage of the sampling sites, particularly in the northern QTP, would cause additional uncertainties in the estimate of Hg storage (Figure S7). In addition, the soil bulk density in eq 6 and NPP in cokriging spatial interpolation are associated with uncertainties which have not yet been well quantified. Furthermore, although human activities are largely absent in the QTP, anthropogenic Hg emissions exist in the large cities of QTP. For example, the rainfall Hg concentration

https://doi.org/10.1021/acs.est.2c09610
Environ. Sci. Technol. 2023, 57, 5903−5912

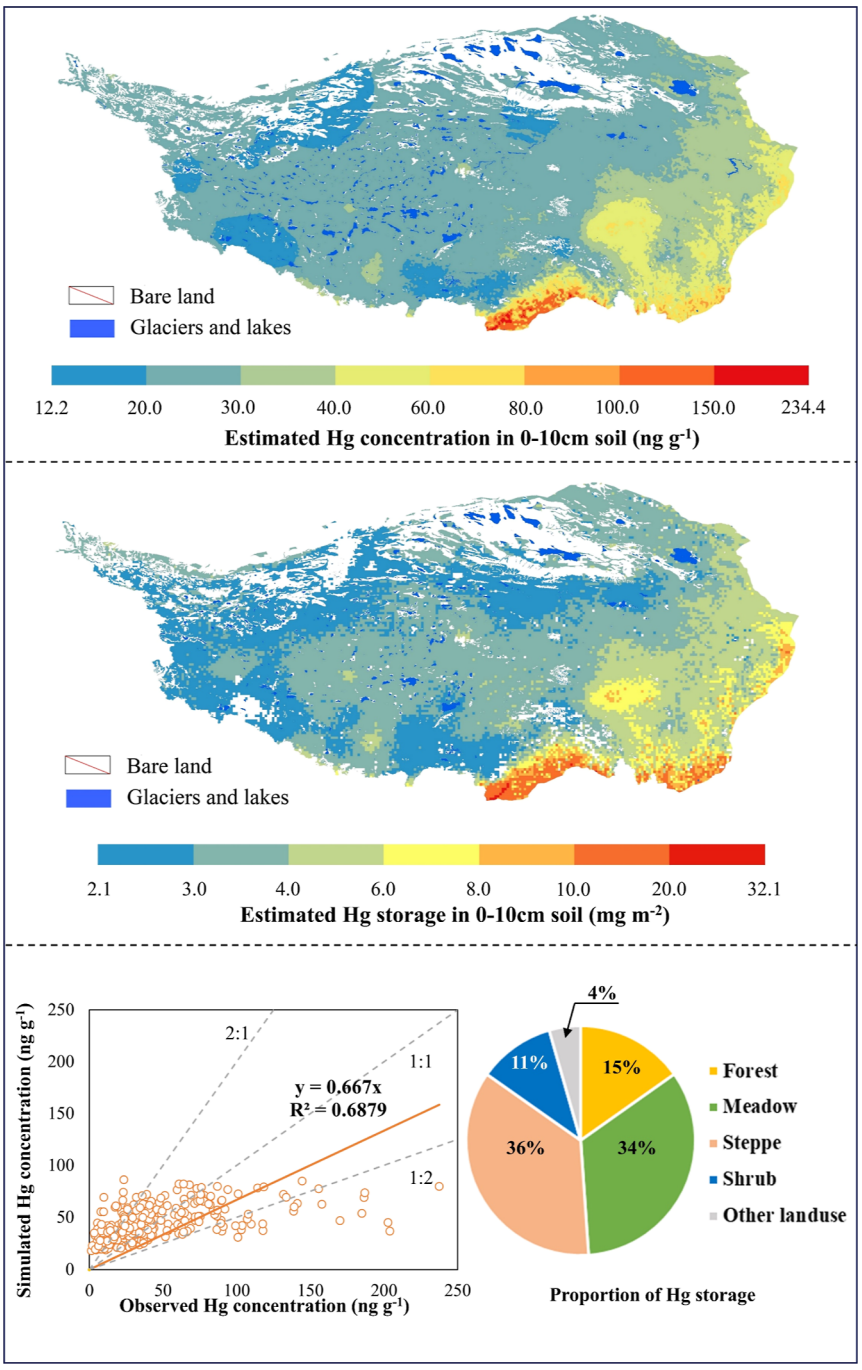

Figure 5. Simulated Hg concentration and storage in surface 0−10 cm soil of the QTP. The scatterplot of observations versus simulated values. The sector chart shows the proportion of Hg storage in the 0−10 cm soil profile for terrestrial biomes in the QTP.

in the city of Lhasa is significantly higher than those found at remote sites.[55,57] Although the influence of local anthropogenic emission was not considered in this study, the impact of man-made emissions should be small over the entire QTP given the total Hg emission in the QTP being lower than 5 Mg yr^{-1}.[69] Finally, the heterogeneities of sampling sites, omission of anthropogenic impact in the QTP (e.g., grazing activities and traffic emission),[10] and permafrost degradation[70] also would induce uncertainties in the estimate of Hg storage in the soil of QTP.

4. ENVIRONMENTAL IMPLICATIONS

In this study, we highlight the collective impact of climate- and vegetation-induced deposition of atmospheric Hg^0 on the Hg accumulation and spatial distribution of soil Hg in the QTP. The Hg storage in surface soil of the QTP is estimated to be 8200 ± 3292 Mg at 0−10 cm depth. The spatial distribution of surface soil Hg presented in this study provides a critical database for estimating the quantity of soil Hg emission, lateral Hg flux, and for assessing ecological risk caused by Hg accumulation in the QTP.[71] The QTP has been experiencing more rapid changes in temperature than the global average, and biomes in the QTP represent one of ecosystems most

https://doi.org/10.1021/acs.est.2c09610
Environ. Sci. Technol. 2023, 57, 5903−5912

affected by global warming.[72] The accelerated warming, wetting, and thawing of permafrost and glaciers over the QTP significantly increase biomass production and vegetation covers with an average rate of increase of NDVI by 0.001 yr^{-1} from 1980 to 2020.[73] Using the correlation between NDVI and soil Hg pool (Figure S8) in this study, we estimated a ~16.5 Mg yr^{-1} Hg storage increase in the surface 0−10 cm soil on the QTP caused by the increase of global warming-induced vegetative production during last 40 years. However, on the other side, the accelerated Hg re-emission from permafrost caused by global warming over the QTP[68,74] could alter the regional Hg cycles and offset the atmospheric Hg sink through vegetation succession. Additionally, permafrost degradation in the QTP can increase the Hg release into aquatic ecosystems via soil erosion and lateral transport and enhance the Hg bioaccumulation and transport in the food web.[8,70] Furthermore, a reduction in anthropogenic Hg emissions decreases atmospheric Hg deposition under the implementation of the Minamata Convention on Mercury, as have been observed in the northern hemisphere remote sites.[75,76] Therefore, there are large knowledge gaps regarding the Hg mass balance over the QTP given the complex interactions among the future scenarios of anthropogenic emissions and global warming. More studies are needed on the Hg biogeochemical processes between the air−soil interface in response to global warming in the QTP.

■ ASSOCIATED CONTENT

Supporting Information

The Supporting Information is available free of charge at https://pubs.acs.org/doi/10.1021/acs.est.2c09610.

Hg isotopic model setup; data of soil Hg concentration, location, NDVI, NPP, annual precipitation, and SOC content in this study; PCA component 1 of NDVI and NPP for SEM fitted on the Hg and atmospheric Hg concentrations; density of coefficient of variation for Hg concentration during sampling processes; distribution of sampling locations; correlations of Hg concentration in surface soil to latitude, longitude, altitude, NPP, NDVI, SOC, and annual precipitation; correlation of Hg concentration in surface soil to altitude in forested areas; and spatial distribution of four types of vegetation covered soil in the QTP (PDF)

■ AUTHOR INFORMATION

Corresponding Author

Xun Wang − *State Key Laboratory of Environmental Geochemistry, Institute of Geochemistry, Chinese Academy of Sciences, Guiyang 550081, China;* orcid.org/0000-0002-7407-8965; Email: wangxun@mail.gyig.ac.cn

Authors

Nantao Liu − *State Key Laboratory of Environmental Geochemistry, Institute of Geochemistry, Chinese Academy of Sciences, Guiyang 550081, China; College of Resources and Environment, Southwest University, Chongqing 400715, China*

Xinyuan Cai − *State Key Laboratory of Environmental Geochemistry, Institute of Geochemistry, Chinese Academy of Sciences, Guiyang 550081, China; University of Chinese Academy of Sciences, Beijing 100049, China*

Longyu Jia − *State Key Laboratory of Environmental Geochemistry, Institute of Geochemistry, Chinese Academy of Sciences, Guiyang 550081, China*

Wei Yuan − *State Key Laboratory of Environmental Geochemistry, Institute of Geochemistry, Chinese Academy of Sciences, Guiyang 550081, China;* orcid.org/0000-0003-3329-2081

Che-Jen Lin − *Center for Advances in Water and Air Quality, Lamar University, Beaumont, Texas 77710, United States*

Dingyong Wang − *College of Resources and Environment, Southwest University, Chongqing 400715, China;* orcid.org/0000-0003-1157-7617

Xinbin Feng − *State Key Laboratory of Environmental Geochemistry, Institute of Geochemistry, Chinese Academy of Sciences, Guiyang 550081, China*

Complete contact information is available at: https://pubs.acs.org/10.1021/acs.est.2c09610

Notes

The authors declare no competing financial interest.

■ ACKNOWLEDGMENTS

This work was funded by National Natural Science Foundation of China (42122053) and Strategic Priority Research Programs of the Chinese Academy of Sciences, the Pan-Third Pole Environment Study for a Green Silk Road (Pan-TPE, XDA2004050201).

■ REFERENCES

(1) Wang, X.; Yuan, W.; Lin, C.-J.; Feng, X. Mercury cycling and isotopic fractionation in global forests. *Crit. Rev. Environ. Sci. Technol.* **2021**, *52*, 3763−3786.

(2) Lindberg, S.; Bullock, R.; Ebinghaus, R.; Engstrom, D.; Feng, X. B.; Fitzgerald, W.; Pirrone, N.; Prestbo, E.; Seigneur, C. A synthesis of progress and uncertainties in attributing the sources of mercury in deposition. *Ambio* **2007**, *36*, 19−33.

(3) Kang, S.; Zhang, Q.; Qian, Y.; Ji, Z.; Li, C.; Cong, Z.; Zhang, Y.; Guo, J.; Du, W.; Huang, J.; et al. Linking atmospheric pollution to cryospheric change in the Third Pole region: current progress and future prospects. *Natl. Sci. Rev.* **2019**, *6*, 796−809.

(4) Sun, S.; Kang, S.; Huang, J.; Chen, S.; Zhang, Q.; Guo, J.; Liu, W.; Neupane, B.; Qin, D. Distribution and variation of mercury in frozen soils of a high-altitude permafrost region on the northeastern margin of the Tibetan Plateau. *Environ. Sci. Pollut. Res.* **2017**, *24*, 15078−15088.

(5) Huang, J.; Kang, S.; Yin, R.; Guo, J.; Lepak, R.; Mika, S.; Tripathee, L.; Sun, S. Mercury isotopes in frozen soils reveal transboundary atmospheric mercury deposition over the Himalayas and Tibetan Plateau. *Environ. Pollut.* **2020**, *256*, 113432.

(6) Wang, X.; Luo, J.; Yin, R.; Yuan, W.; Lin, C. J.; Sommar, J.; Feng, X.; Wang, H.; Lin, C. Using Mercury Isotopes To Understand Mercury Accumulation in the Montane Forest Floor of the Eastern Tibetan Plateau. *Environ. Sci. Technol.* **2017**, *51*, 801−809.

(7) Gong, P.; Wang, X.-p.; Xue, Y.-g.; Xu, B.-q.; Yao, T.-d. Mercury distribution in the foliage and soil profiles of the Tibetan forest: processes and implications for regional cycling. *Environ. Pollut.* **2014**, *188*, 94−101.

(8) Gu, J.; Pang, Q.; Ding, J.; Yin, R.; Yang, Y.; Zhang, Y. The driving factors of mercury storage in the Tibetan grassland soils underlain by permafrost. *Environ. Pollut.* **2020**, *265*, 115079.

(9) Sun, R.; Sun, G.; Kwon, S. Y.; Feng, X.; Kang, S.; Zhang, Q.; Huang, J.; Yin, R. Mercury biogeochemistry over the Tibetan Plateau: An overview. *Crit. Rev. Environ. Sci. Technol.* **2021**, *51*, 577−602.

(10) An, S.; Liu, N.; Li, X.; Zeng, S.; Wang, X.; Wang, D. Understanding heavy metal accumulation in roadside soils along

major roads in the Tibet Plateau. *Sci. Total Environ.* **2022**, *802*, 149865.
(11) Liu, Y.-R.; Dong, J.-X.; Zhang, Q.-G.; Wang, J.-T.; Han, L.-L.; Zeng, J.; He, J.-Z. Longitudinal occurrence of methylmercury in terrestrial ecosystems of the Tibetan Plateau. *Environ. Pollut.* **2016**, *218*, 1342−1349.
(12) Wang, X.; Yuan, W.; Lu, Z.; Lin, C. J.; Yin, R.; Li, F.; Feng, X. Effects of Precipitation on Mercury Accumulation on Subtropical Montane Forest Floor: Implications on Climate Forcing. *J. Geophys. Res.: Biogeosci.* **2019**, *124*, 959−972.
(13) Obrist, D.; Agnan, Y.; Jiskra, M.; Olson, C. L.; Colegrove, D. P.; Hueber, J.; Moore, C. W.; Sonke, J. E.; Helmig, D. Tundra uptake of atmospheric elemental mercury drives Arctic mercury pollution. *Nature* **2017**, *547*, 201−204.
(14) Jiskra, M.; Wiederhold, J. G.; Skyllberg, U.; Kronberg, R. M.; Hajdas, I.; Kretzschmar, R. Mercury deposition and re-emission pathways in boreal forest soils investigated with Hg isotope signatures. *Environ. Sci. Technol.* **2015**, *49*, 7188−7196.
(15) Demers, J. D.; Blum, J. D.; Zak, D. R. Mercury isotopes in a forested ecosystem: Implications for air-surface exchange dynamics and the global mercury cycle. *Global Biogeochem. Cycles* **2013**, *27*, 222−238.
(16) Zheng, W.; Obrist, D.; Weis, D.; Bergquist, B. A. Mercury isotope compositions across North American forests. *Global Biogeochem. Cycles* **2016**, *30*, 1475−1492.
(17) Fiorentino, J. C.; Enzweiler, J.; Angélica, R. S. Geochemistry of Mercury Along a Soil Profile Compared to Other Elements and to the Parental Rock: Evidence of External Input. *Water, Air, Soil Pollut.* **2011**, *221*, 63−75.
(18) Obrist, D.; Pearson, C.; Webster, J.; Kane, T.; Lin, C.-J.; Aiken, G. R.; Alpers, C. N. A synthesis of terrestrial mercury in the western United States: Spatial distribution defined by land cover and plant productivity. *Sci. Total Environ.* **2016**, *568*, 522−535.
(19) Lu, H.; Shao, Q.; Liu, J.; Wang, J.; Chen, Z. Temporo-spatial Distribution of Summer Precipitationover Qinghai-Tibet Plateau during the Last 44 Years. *Acta Geogr. Sin.* **2007**, *62*, 946−958.
(20) Zhang, Y.; Wang, G.; Wang, Y. Response of biomass spatial pattern of alpine vegetation to climate change in permafrost region of the Qinghai-Tibet Plateau, China. *J. Mt. Sci.* **2010**, *7*, 301−314.
(21) Shi, Z.; Tao, H.; Liu, S.; Liu, B.; Guo, B. Research of freeze-thaw erosion in the Three-River-Source area based on GIS. *Trans. Chin. Soc. Agric. Eng.* **2012**, *28*, 214.
(22) Zhang, C.-L.; Li, Q.; Shen, Y.-P.; Zhou, N.; Wang, X.-S.; Li, J.; Jia, W.-R. Monitoring of aeolian desertification on the Qinghai-Tibet Plateau from the 1970s to 2015 using Landsat images. *Sci. Total Environ.* **2018**, *619−620*, 1648−1659.
(23) Sheng, J.; Wang, X.; Gong, P.; Tian, L.; Yao, T. Heavy metals of the Tibetan top soils: level, source, spatial distribution, temporal variation and risk assessment. *Environ. Sci. Pollut. Res. Int.* **2012**, *19*, 3362−3370.
(24) Yu, B.; Yang, L.; Liu, H.; Xiao, C.; Bu, D.; Zhang, Q.; Fu, J.; Zhang, Q.; Cong, Z.; Liang, Y.; et al. Tracing the Transboundary Transport of Mercury to the Tibetan Plateau Using Atmospheric Mercury Isotopes. *Environ. Sci. Technol.* **2022**, *56*, 1568−1577.
(25) Fu, X. W.; Feng, X.; Liang, P.; Deliger; Zhang, H.; Ji, J.; Liu, P. Temporal trend and sources of speciated atmospheric mercury at Waliguan GAW station, Northwestern China. *Atmos. Chem. Phys.* **2012**, *12*, 1951−1964.
(26) Zhang, H.; Fu, X. W.; Yu, B.; Li, B. X.; Liu, P.; Zhang, G. Q.; Zhang, L. M.; Feng, X. B. Speciated atmospheric mercury at the Waliguan Global Atmosphere Watch station in the northeastern Tibetan Plateau: implication of dust-related sources for particulate bound mercury. *Atmos. Chem. Phys.* **2021**, *21*, 15847−15859.
(27) Zhang, H.; Fu, X. W.; Lin, C. J.; Wang, X.; Feng, X. B. Observation and analysis of speciated atmospheric mercury in Shangri-La, Tibetan Plateau, China. *Atmos. Chem. Phys.* **2015**, *15*, 653−665.
(28) Sonke, J. E.; Blum, J. D. Advances in mercury stable isotope biogeochemistry. *Chem. Geol.* **2013**, *336*, 1−4.
(29) Yin, R.; Feng, X.; Li, X.; Yu, B.; Du, B. Trends and advances in mercury stable isotopes as a geochemical tracer. *Trends Environ. Anal. Chem.* **2014**, *2*, 1−10.
(30) Tsui, M. T.-K.; Blum, J. D.; Kwon, S. Y. Review of stable mercury isotopes in ecology and biogeochemistry. *Sci. Total Environ.* **2020**, *716*, 135386.
(31) Wang, X.; Luo, J.; Yuan, W.; Lin, C.-J.; Wang, F.; Liu, C.; Wang, G.; Feng, X. Global warming accelerates uptake of atmospheric mercury in regions experiencing glacier retreat. *Proc. Natl. Acad. Sci.* **2020**, *117*, 2049−2055.
(32) Rose, C. H.; Ghosh, S.; Blum, J. D.; Bergquist, B. A. Effects of ultraviolet radiation on mercury isotope fractionation during photo-reduction for inorganic and organic mercury species. *Chem. Geol.* **2015**, *405*, 102−111.
(33) Zheng, W.; Hintelmann, H. Mercury isotope fractionation during photoreduction in natural water is controlled by its Hg/DOC ratio. *Geochim. Cosmochim. Acta* **2009**, *73*, 6704−6715.
(34) Zheng, W.; Hintelmann, H. Isotope fractionation of mercury during its photochemical reduction by low-molecular-weight organic compounds. *J. Phys. Chem. A* **2010**, *114*, 4246−4253.
(35) Bergquist, B. A.; Blum, J. D. Mass-Dependent and -Independent Fractionation of Hg Isotopes by Photoreduction in Aquatic Systems. *Science* **2007**, *318*, 417−420.
(36) Zheng, W.; Hintelmann, H. Nuclear field shift effect in isotope fractionation of mercury during abiotic reduction in the absence of light. *J. Phys. Chem. A* **2010**, *114*, 4238−4245.
(37) Gratz, L. E.; Keeler, G. J.; Blum, J. D.; Sherman, L. S. Isotopic Composition and Fractionation of Mercury in Great Lakes Precipitation and Ambient Air. *Environ. Sci. Technol.* **2010**, *44*, 7764−7770.
(38) Chen, J.; Hintelmann, H.; Feng, X.; Dimock, B. Unusual fractionation of both odd and even mercury isotopes in precipitation from Peterborough, ON, Canada. *Geochim. Cosmochim. Acta* **2012**, *90*, 33−46.
(39) Yuan, W.; Wang, X.; Lin, C.-J.; Sommar, J. O.; Wang, B.; Lu, Z.; Feng, X. Quantification of Atmospheric Mercury Deposition to and Legacy Re-emission from a Subtropical Forest Floor by Mercury Isotopes. *Environ. Sci. Technol.* **2021**, *55*, 12352−12361.
(40) Walkley, A. A critical examination of a rapid method for determining organic carbon in soils effect of variations in digestion conditions and of inorganic soil constituents. *Soil Sci.* **1947**, *63*, 251−264.
(41) Sun, R. Y.; Enrico, M.; Heimburger, L. E.; Scott, C.; Sonke, J. E. A double-stage tube furnace-acid-trapping protocol for the pre-concentration of mercury from solid samples for isotopic analysis. *Anal. Bioanal. Chem.* **2013**, *405*, 6771−6781.
(42) United States Environmental Protection Agency *Method 1631, Revision E: Mercury in Water by Oxidation, Purge and Trap, and Cold Vapor Atomic Fluorescence Spectrometry*, 2002.
(43) Estrade, N.; Carignan, J.; Sonke, J. E.; Donard, O. F. X. Measuring Hg Isotopes in Bio-Geo-Environmental Reference Materials. *Geostand. Geoanal. Res.* **2010**, *34*, 79−93.
(44) Yuan, W.; Wang, X.; Lin, C.-J.; Wu, C.; Zhang, L.; Wang, B.; Sommar, J.; Lu, Z.; Feng, X. Stable Mercury Isotope Transition during Postdepositional Decomposition of Biomass in a Forest Ecosystem over Five Centuries. *Environ. Sci. Technol.* **2020**, *54*, 8739−8749.
(45) Xia, S.; Yuan, W.; Lin, L.; Yang, X.; Feng, X.; Li, X.; Liu, X.; Chen, P.; Zeng, S.; Wang, D.; et al. Latitudinal gradient for mercury accumulation and isotopic evidence for post-depositional processes among three tropical forests in Southwest China. *J. Hazard. Mater.* **2022**, *429*, 128295.
(46) Wang, X.; Yuan, W.; Lin, C.-J.; Wang, D.; Luo, J.; Xia, J.; Zhang, W.; Wang, F.; Feng, X. Root uptake dominates mercury accumulation in permafrost plants of Qinghai-Tibet Plateau. *Commun. Earth Environ.* **2022**, *3*, 287.
(47) mingjun, D. Temperature and precipitation grid data of the Qinghai Tibet Plateau and its surrounding areas in 1998-2017Grid data of annual temperature and annual precipitation on the Tibetan

https://doi.org/10.1021/acs.est.2c09610
Environ. Sci. Technol. 2023, 57, 5903−5912

Plateau and its surrounding areas during 1998-2017. *National Tibetan Plateau Data*; National Tibetan Plateau Data Center, 2019.
(48) Fei, Y. Vegetation Index (NDVI) data of Tibetan Plateau. *National Tibetan Plateau Data*; National Tibetan Plateau Data Center, 2019.
(49) Juntao, Z. A dataset of net primary productivity of vegetation on the Qinghai-Tibet Plateau (2001-2020). *National Tibetan Plateau Data*; National Tibetan Plateau Data Center, 2022.
(50) Food and Agriculture Organization of the United Nations. Dataset of soil texture on the Qinghai-Tibet Plateau (2010). *National Tibetan Plateau Data*; National Tibetan Plateau Data Center, 2019.
(51) Wang, X.; Yuan, W.; Lin, C.-J.; Zhang, L.; Zhang, H.; Feng, X. Climate and Vegetation As Primary Drivers for Global Mercury Storage in Surface Soil. *Environ. Sci. Technol.* **2019**, *53*, 10665−10675.
(52) Yang, H.; Battarbee, R. W.; Turner, S. D.; Rose, N. L.; Derwent, R. G.; Wu, G.; Yang, R. Historical Reconstruction of Mercury Pollution Across the Tibetan Plateau Using Lake Sediments. *Environ. Sci. Technol.* **2010**, *44*, 2918−2924.
(53) Wang, X.; Lin, C.-J.; Lu, Z.; Zhang, H.; Zhang, Y.; Feng, X. Enhanced accumulation and storage of mercury on subtropical evergreen forest floor: Implications on mercury budget in global forest ecosystems. *J. Geophys. Res.: Biogeosci.* **2016**, *121*, 2096−2109.
(54) Zhang, H.; Yin, R. S.; Feng, X. B.; Sommar, J.; Anderson, C. W. N.; Sapkota, A.; Fu, X. W.; Larssen, T. Atmospheric mercury inputs in montane soils increase with elevation: evidence from mercury isotope signatures. *Sci. Rep.* **2013**, *3*, 3322.
(55) Huang, J.; Kang, S. C.; Wang, S. X.; Wang, L.; Zhang, Q. G.; Guo, J. M.; Wang, K.; Zhang, G. S.; Tripathee, L. Wet deposition of mercury at Lhasa, the capital city of Tibet. *Sci. Total Environ.* **2013**, *447*, 123−132.
(56) Huang, J.; Kang, S. C.; Zhang, Q. G.; Guo, J. M.; Sillanpaa, M.; Wang, Y. J.; Sun, S. W.; Sun, X. J.; Tripathee, L. Characterizations of wet mercury deposition on a remote high-elevation site in the southeastern Tibetan Plateau. *Environ. Pollut.* **2015**, *206*, 518−526.
(57) Huang, J.; Kang, S. C.; Zhang, Q. G.; Yan, H. Y.; Guo, J. M.; Jenkins, M. G.; Zhang, G. S.; Wang, K. Wet deposition of mercury at a remote site in the Tibetan Plateau: Concentrations, speciation, and fluxes. *Atmos. Environ.* **2012**, *62*, 540−550.
(58) Jiang, Z.; Bian, H.; Xu, L.; Li, M.; He, N. Effects of pulse precipitation on soil organic matter mineralization in forests: spatial variation and controlling factors. *J. Plant Ecol.* **2021**, *14*, 970−980.
(59) Guan, S.; An, N.; Zong, N.; He, Y.; Shi, P.; Zhang, J.; He, N. Climate warming impacts on soil organic carbon fractions and aggregate stability in a Tibetan alpine meadow. *Soil Biol. Biochem.* **2018**, *116*, 224−236.
(60) Obrist, D.; Johnson, D. W.; Lindberg, S. E. Mercury concentrations and pools in four Sierra Nevada forest sites, and relationships to organic carbon and nitrogen. *Biogeosciences* **2009**, *6*, 765−777.
(61) Skyllberg, U.; Bloom, P. R.; Qian, J.; Lin, C.-M.; Bleam, W. F. Complexation of Mercury(II) in Soil Organic Matter: EXAFS Evidence for Linear Two-Coordination with Reduced Sulfur Groups. *Environ. Sci. Technol.* **2006**, *40*, 4174−4180.
(62) Wang, X.; Yuan, W.; Lin, C. J.; Luo, J.; Wang, F.; Feng, X.; Fu, X.; Liu, C. Underestimated Sink of Atmospheric Mercury in a Deglaciated Forest Chronosequence. *Environ. Sci. Technol.* **2020**, *54*, 8083−8093.
(63) Yuan, W.; Sommar, J.; Lin, C.-J.; Wang, X.; Li, K.; Liu, Y.; Zhang, H.; Lu, Z.; Wu, C.; Feng, X. Stable Isotope Evidence Shows Re-emission of Elemental Mercury Vapor Occurring after Reductive Loss from Foliage. *Environ. Sci. Technol.* **2019**, *53*, 651−660.
(64) Kwon, S. Y.; Blum, J. D.; Yin, R.; Tsui, M. T. K.; Yang, Y. H.; Choi, J. W. Mercury stable isotopes for monitoring the effectiveness of the Minamata Convention on Mercury. *Earth-Sci. Rev.* **2020**, *203*, 103111.
(65) Blum, J. D.; Sherman, L. S.; Johnson, M. W. Mercury Isotopes in Earth and Environmental Sciences. *Annu. Rev. Earth Planet. Sci.* **2014**, *42*, 249−269.
(66) Kang, S.; Huang, J.; Wang, F.; Zhang, Q.; Zhang, Y.; Li, C.; Wang, L.; Chen, P.; Sharma, C. M.; Li, Q.; et al. Atmospheric Mercury Depositional Chronology Reconstructed from Lake Sediments and Ice Core in the Himalayas and Tibetan Plateau. *Environ. Sci. Technol.* **2016**, *50*, 2859−2869.
(67) Ci, Z.; Peng, F.; Xue, X.; Zhang, X. Air−surface exchange of gaseous mercury over permafrost soil: an investigation at a high-altitude (4700 m a.s.l.) and remote site in the central Qinghai−Tibet Plateau. *Atmos. Chem. Phys.* **2016**, *16*, 14741−14754.
(68) Sun, S.; Ma, M.; He, X.; Obrist, D.; Zhang, Q.; Yin, X.; Sun, T.; Huang, J.; Guo, J.; Kang, S.; et al. Vegetation Mediated Mercury Flux and Atmospheric Mercury in the Alpine Permafrost Region of the Central Tibetan Plateau. *Environ. Sci. Technol.* **2020**, *54*, 6043−6052.
(69) Liu, K.; Wu, Q.; Wang, L.; Wang, S.; Liu, T.; Ding, D.; Tang, Y.; Li, G.; Tian, H.; Duan, L.; et al. Measure-Specific Effectiveness of Air Pollution Control on China's Atmospheric Mercury Concentration and Deposition during 2013-2017. *Environ. Sci. Technol.* **2019**, *53*, 8938−8946.
(70) Mu, C.; Schuster, P. F.; Abbott, B. W.; Kang, S.; Guo, J.; Sun, S.; Wu, Q.; Zhang, T. Permafrost degradation enhances the risk of mercury release on Qinghai-Tibetan Plateau. *Sci. Total Environ.* **2020**, *708*, 135127.
(71) Liu, M.; Zhang, Q.; Luo, Y.; Mason, R. P.; Ge, S.; He, Y.; Yu, C.; Sa, R.; Cao, H.; Wang, X.; et al. Impact of Water-Induced Soil Erosion on the Terrestrial Transport and Atmospheric Emission of Mercury in China. *Environ. Sci. Technol.* **2018**, *52*, 6945−6956.
(72) Zhang, G.; Yao, T.; Xie, H.; Qin, J.; Ye, Q.; Dai, Y.; Guo, R. Estimating surface temperature changes of lakes in the Tibetan Plateau using MODIS LST data. *J. Geophys. Res.: Atmos.* **2014**, *119*, 8552−8567.
(73) Wang, Y.; Lv, W.; Xue, K.; Wang, S.; Zhang, L.; Hu, R.; Zeng, H.; Xu, X.; Li, Y.; Jiang, L.; et al. Grassland changes and adaptive management on the Qinghai−Tibetan Plateau. *Nat. Rev. Earth Environ.* **2022**, *3*, 668−683.
(74) Ci, Z.; Peng, F.; Xue, X.; Zhang, X. Permafrost Thaw Dominates Mercury Emission in Tibetan Thermokarst Ponds. *Environ. Sci. Technol.* **2020**, *54*, 5456−5466.
(75) Zhang, Y.; Jacob, D. J.; Horowitz, H. M.; Chen, L.; Amos, H. M.; Krabbenhoft, D. P.; Slemr, F.; St Louis, V. L.; Sunderland, E. M. Observed decrease in atmospheric mercury explained by global decline in anthropogenic emissions. *Proc. Natl. Acad. Sci.* **2016**, *113*, 526−531.
(76) Tang, Y.; Wang, S.; Wu, Q.; Liu, K.; Wang, L.; Li, S.; Gao, W.; Zhang, L.; Zheng, H.; Li, Z.; et al. Recent decrease trend of atmospheric mercury concentrations in East China: the influence of anthropogenic emissions. *Atmos. Chem. Phys.* **2018**, *18*, 8279−8291.

https://doi.org/10.1021/acs.est.2c09610
Environ. Sci. Technol. 2023, 57, 5903−5912